APPLICATION OF ARTIFICIAL NEURAL NETWORKS FOR RECONSTRUCTION OF VECTOR MAGNETIC FIELD FROM SINGLE-COMPONENT DATA

© 2025 R. A. Rytov*, V. G. Petrov**

Pushkov Institute of Terrestrial Magnetism, Ionosphere and Radio Wave Propagation, Russian Academy of Sciences, IZMIRAN, Troitsk, Moscow, Russia

**e-mail: ruslan.rytov2017@ya.ru*

***e-mail: vgpetrov2018@mail.ru*

Received April 12, 2024

Revised May 29, 2024

Accepted July 25, 2024

Abstract. In this work the problem of reconstructing the vector anomalous magnetic field from single-component data was solved by means of artificial neural networks. For training an artificial neural network a database of anomalous magnetic field components B_x, B_y, B_z was created using a set of point magnetic dipoles lying under the field measurement plane. Using a synthetic example, the work of a trained neural network was shown in comparison with a well-known numerical algorithm for restoring a vector field from data of one component. Further, according to the data of the vertical component of the anomalous geomagnetic field the horizontal components of the anomalous geomagnetic field were restored using artificial neural networks in the territory of 58 – 85º E, 52 – 74º N with a grid step of 2 arc minutes.

Keywords: *artificial neural networks, anomalous magnetic field, vector magnetic field, computer modeling*

DOI: 10.31857/S00167940250613e2

1. INTRODUCTION

Anomalous magnetic field vector models are widely used for geophysics, navigation, and directional drilling applications [Buchanan et al., 2013; Kaji et al., 2019]. However, the number of modular anomalous field data exceeds the number of vector measurements. Therefore, in order to

obtain a highly accurate vector magnetic field model, special methods are used to calculate the vector anomalous magnetic field from the known single-component anomalous magnetic field data.

Examples of such methods are the magnetic potential method [Lourenco and Morrison, 1973; Kolesova and Cherkaeva, 1987] and the magnetic dipole method [Montesinos et al., 2016; Kaftan, 2017]. In the magnetic potential method, the field components are described by double Fourier series whose coefficients are related through the anomalous magnetic field potential. However, this method requires that the magnetic anomaly is completely within the measurement domain [Lourenco and Morrison, 1973; Kolesova and Cherkaeva, 1987]. With the dipole method, the desired vector field is calculated, based on the known component of the anomalous field, using a set of fictitious point dipoles whose positions are selected by trial and error under the scanning plane of the anomalous field. However, the running time of the dipole method increases rapidly with increasing number of dipoles and measurement points of the anomalous magnetic field.

The application of artificial neural networks is effective for fast processing of a large volume of digital images. Artificial neural networks are widely used for applications in computer vision and image classification [Krizhevsky et al., 2012]. Neural networks trained on physical process data have been used to model magnetic fields and to interpolate and extend magnetic fields measured on a sparse grid [Coskun et al., 2022; Pollok et al., 2021; Pollok et al., 2023]. In some cases, the trained neural network shows higher accuracy compared to traditional numerical algorithms [Coskun et al., 2022; Pollok et al., 2021].

In this paper, a new method of vector magnetic field reconstruction using artificial neural networks is proposed. The neural network takes as input the data of vertical B_z -component of anomalous field of dimensionality 40 × 40 pixels, and then reconstructs the components in the plane B_x and B_y. To train the developed neural network, a database containing 50000 random anomalous magnetic fields was created using the total field of point magnetic dipoles. The developed neural network was compared with the known numerical method of vector field reconstruction [Lourenco and Morrison, 1973; Kolesova and Cherkaeva, 1987]. The performance of the neural network was also verified using the data of the vertical component of the anomalous field obtained with the IGRF-13 [Alken et al., 2021] and EMM2017 [Maus, 2010; The National Centers for Environmental Information, 2018] models over the area 58 - 85º E, 52 - 74º N with a grid spacing of 2 angular minutes.

2. METHOD DESCRIPTION

2.1 Neural network architecture

The schematic of the developed artificial neural network is shown in Fig. 1. The known distribution of the vertical component of the anomalous field B_z of dimension 40 × 40 pixels is input to the neural network. A dense neural network containing an input layer, an inner layer and an output layer of 40 × 40 neurons is used for preliminary coarse calculation. Then the results of the coarse calculation of the anomalous field components are input to the refinement neural network. The refinement is performed using a convolutional neural network with an input layer, an output layer and two inner layers containing 40 × 40 neurons. A linear neuron activation function was used in the developed model.

Fig. 1.

The neural network was implemented using the *tensorflow* library [Abadi et al., 2016]. The choice of *tensorflow* library is justified by high performance, flexibility and convenience of neural network development. *Adam's* stochastic gradient descent algorithm [Kingma et al., 2014] was used to train the neural network.

In order to train the neural network and further estimate the accuracy of magnetic field reconstruction, it is necessary to specify the mismatch function. There are many well-known non-convexity functions, some of which are implemented in the *tensorflow* package, e.g. mean square of deviation, mean modulus of deviation, etc. There are also more advanced functions, such as the *PE* function [Barkhatov et al., 2017]. The choice of a particular incoherence function for training a neural network depends on the type of input data and can be selected experimentally. In this paper, for simplicity, we have chosen the RMS error function of the form

$$L = \frac{1}{N}\sum_i \frac{\left(B_i - B_i^R\right)^2}{\left\langle B^2 \right\rangle}, \qquad (1)$$

where B_i is the known field at point *i*, B_i^R is the reconstructed field at point *i*, $\left\langle B^2 \right\rangle$ is the mean square of the known anomalous field, *N* is the total number of measurement points.

The training database consists of 50000 random components of the anomalous magnetic field B_x, B_y, B_z, of which 45000 components were used to train the artificial neural network, 5000 components were used to validate the training process of the neural network. During the training process, the non-convexity reached values of $L < 4 \cdot 10^{-3}$.

2.2 Direct modeling of the anomalous field

Point dipoles were used to model the anomalous magnetic field because the magnetic field of a magnetized body at distances greater than its size is equivalent to the field of a point dipole. The field of a point magnetic dipole is determined by the well-known formula [Yanovsky, 1978]

$$\vec{B}(\vec{r}) = \frac{3\vec{r}(\vec{m},\vec{r})}{|\vec{r}|^5} - \frac{\vec{m}}{|\vec{r}|^3}, \qquad (2)$$

where $\vec{r}$ is the vector from the dipole location point to the measurement point, $\vec{m}$ is the magnetic moment of the dipole in the Cartesian coordinate system. The anomalous magnetic field is modeled using a random distribution of 1 - 400 point magnetic dipoles. The components of the anomalous magnetic field are then calculated in the plane at some height above the point dipoles and entered into the database. The numerical values of the anomalous field components are normalized so that they lie in the range [-1, 1].

2.3 Training of the neural network

Training of the developed neural network was conducted on a personal computer with *Intel Core* i7-9700 processor and *NVIDIA GeForce GTX* 950 video card. In order to utilize 2 Gb of free memory of the video card, the input data for training, with the total size of a little more than 2 Gb, was divided into equal parts of 1 Gb each. Then the training was performed on each data series until the moment when the non-convexity on the validation sample becomes greater than the non-convexity of the training sample. An example plot of the dynamics of the linkage function during training in logarithmic scale is shown in Fig. 2.

Fig. 2.

Fig. 2 shows the process of decreasing the value of the mismatch function for training data and for validation data. In order to avoid overtraining the neural network, the training process was stopped if the non-convexity of the validation sample started to increase relative to the non-convexity of the training sample [Ying, 2019]. This point is shown in Fig. 2 with an arrow, it corresponds to approximately 80 epoch number.

3. SYNTHETIC EXAMPLE

The trained neural network was validated using test anomalous magnetic fields that were not part of the shared database during training. Fig. 3 shows, for a specific example, the result of the trained neural network in comparison with the numerical algorithm for recovering the horizontal components of the anomalous magnetic field, which is described in detail in [Lourenco and Morrison, 1973].

Fig. 3.

Figs. 3*a*-3*b* show the results of recovery of the horizontal B_x and B_y components of the anomalous field from the data of the vertical B_z-component using the numerical algorithm. Figs. 3*c*

- 3*d* show the results of the trained neural network for the same input data. The series in Fig. 3 show the original components B_x and B_y, the reconstructed components $B_x^{asst.}$ and $B_y^{asst.}$, and the difference between the original and reconstructed magnetic field components obtained using the numerical algorithm and the artificial neural network.

Fig. 3 shows that in the case of the numerical algorithm operation, the discrepancy calculated by formula (1) takes the values $L = 0.1067$ and $L = 0.1606$ for the components B_x and B_y, respectively. For the neural network results, the error takes the values of $L = 0.0031$ and $L = 0.0018$ for the components B_x and B_y, respectively. Figs. 3*a* - 3*b* show that in the case of the numerical algorithm, the main contribution to the error is due to edge effects, which are absent in the neural network results, as shown in Figs. 3*c* - 3*d*. Edge effects arise when the magnetic anomaly does not enter the entire study area [Lourenco and Morrison, 1973; Kolesova and Cherkaeva, 1987].

To reduce the overall mismatch, the edge 10 px of each image is removed and the mismatch is computed in the region 20 × 20 px shown in Fig. 3. In this case, for the numerical algorithm, the bias takes the values of $L = 0.0082$ and $L = 0.0112$ for B_x and B_y components, respectively, while in the case of the trained neural network, the bias is $L = 4.2 \cdot 10^{-4}$ and $L = 2.7 \cdot 10^{-4}$ for B_x and B_y components, respectively.

Next, we compared the average non-convexity of the results of the numerical algorithm and the trained neural network on 1000 random distributions of the anomalous magnetic field, which were not included in the database when the neural network was trained. Cases where the magnetic anomaly is not entirely within the considered area were also included in the sample. The mismatch was calculated both for the whole image 40 × 40 px and for images without edge pixels, 20 × 20 px. The results of the comparison performed are shown in Table 1.

Table 1.

The results shown in Table 1 show that the artificial neural network has, on average, better accuracy in the sense of the mismatch function (1) compared to the known numerical algorithm. If we also take into account the influence of edge effects and discard 10 pixels from each edge of the image, the accuracy of vector field reconstruction increases significantly for both methods, but even in this case the neural network shows slightly better results.

3.1 Effect of noise

Next, the performance of the artificial neural network was tested on noisy data. The results of the validation are shown in Fig. 4.

Fig. 4.

To model white noise, a random number in the range [-0.5, 0.5] was added to each pixel value of the vertical component B_z, as shown in Fig. 4*a*. The true in-plane components, B_x and B_y are also

shown here. From a given noisy component B_z, the in-plane components B_x and B_y were reconstructed using an artificial neural network, Fig. 4*b*, and using a numerical algorithm, Fig. 4*c*.

The difference between the true components and the reconstructed components is shown in Fig. 4*b* for the artificial neural network and in Fig. 4*c* for the numerical algorithm. In the case of the neural network, the non-convexity takes values of $L = 0.0578$ for the B_x component and $L = 0.0464$ for the B_y-component. For the numerical algorithm, the incoherence takes the values $L = 0.4613$ for the B_x-component and $L = 0.6579$ for the B_y-component.

Further, as in the previous section, we compared the average mismatch of the results of the numerical algorithm and the trained neural network on 1000 random noisy distributions of the vertical component of the anomalous magnetic field. The mismatch was also calculated both for the whole image 40 × 40 px and for images without edge pixels, 20 × 20 px. The results of this comparison are shown in Table 2.

Table 2.

The results in Table 2 show that the artificial neural network on average shows better robustness to noise in the input data. Thus, in the case of numerical algorithm, the average bias for B_x-and B_y-components of the anomalous field is $L = 0.7493$ and $L = 0.8122$, respectively. For the artificial neural network, the average incoherence for the B_x- and B_y-component of the anomalous field is $L = 0.0733$ and $L = 0.0680$, respectively. If the edge pixels are discarded, for the numerical algorithm, the bias takes the values of $L = 0.1496$ and $L = 0.1895$ for the B_x and B_y components, respectively, while for the artificial neural network, the bias takes the values of $L = 0.0122$ and $L = 0.0126$ for the B_x and B_y components, respectively.

4. CALCULATION OF THE ANOMALOUS GEOMAGNETIC FIELD COMPONENTS FROM THE VERTICAL COMPONENT DATA

The artificial neural network was tested on a large amount of anomalous geomagnetic field data. Using the IGRF-13 and EMM2017 models, vertical component data of the anomalous field over the region 58 - 85º E, 52 - 74º N with a grid spacing of 2 angular minutes at an altitude of 4 km were obtained as shown in Fig. 5.

Fig. 5.

The data of the main geomagnetic field produced by currents in the Earth's core were obtained from the IGRF-13 model. The data of the total geomagnetic field were obtained from the EMM2017 model. The EMM2017 model allows obtaining both the main magnetic field and the field of magnetic anomalies, which are created by rocks in the Earth's crust, to an accuracy of 51 km [The National Centers for Environmental Information, 2018]. To obtain exactly the anomalous magnetic field, the difference between the EMM2017 full field model data and the IGRF-13 main field was calculated. The calculation was performed using the following parameters: year 2020,

altitude 4 km above sea level, longitude 58 - 85º E in 0.03 degree increments, latitude 52 - 74º N in 0.03 degree increments. The results of reconstructing the in-plane components of the anomalous magnetic field are shown in Fig. 6.

Fig. 6.

The anomalous field on the geographic coordinate grid was transformed into a kilometer uniform grid with a distance between neighboring points of 2 km, totaling 1386 × 1286 points. To process the image using an artificial neural network, the resulting vertical component map was randomly partitioned into 50000 intersecting patches with dimensions of 40 × 40 pixels.

Then, each section was processed by the neural network, and 10 edge pixels of each image were removed to reduce the influence of edge effects. Finally, anomalous magnetic field maps of the original size were generated from small 20 × 20 pixel plots, which contain data on the reconstructed B_x and B_y components of the anomalous magnetic field.

The calculation was performed on a personal computer; the time of processing 50000 images of 40 × 40 pixels using an artificial neural network does not exceed 1 min when the calculation is performed on a CPU. Map transformations from geographic coordinates to kilometer coordinates and back were performed using interpolation algorithms implemented in the open scipy library [Virtanen et. al., 2020].

The series in Figs. 6*a* - 6*b* show the true field components B_x and B_y, obtained from the EMM model, the reconstructed components $B_x^{asc.}$ and B_y^{asc} using an artificial neural network, and the difference between the true and reconstructed components of the anomalous magnetic field. Thus, for the B_x component, the discrepancy function takes the value $L = 0.0931$, and for the B_y component, the discrepancy function takes the value $L = 0.0252$.

In the region of the highest intensity of magnetic anomalies, $|B_x| = 1642$ nTl, $|B_y| = 1853$ nTl, the error takes values of 170 nTl and 98 nTl, respectively. In the high latitude region, the error for the B_x component is the largest, as shown in Fig. 6a. This may be due to the large extent of the anomalies themselves in this region, about 400 px as shown in Fig. 5*b*, compared to the extent of the neural network input image, 40 px.

5. CONCLUSION

In this paper, an artificial neural network model was developed to reconstruct the vector anomalous magnetic field from vertical field component data. The neural network contains a dense input layer for preliminary coarse calculation, the results of which are further refined using a convolutional neural network. The developed neural network was trained on data generated using a random distribution of fictitious point magnetic dipoles, which were used to model the anomalous magnetic field over the earth's surface.

The neural network showed on average better results when compared to a known numerical scheme for recovering the in-plane magnetic field components. The trained neural network recovers field components with smaller marginal errors for cases where the magnetic anomaly is not entirely within the desired region. The neural network also showed robustness to noise in the input data.

The results of vector field reconstruction based on IGRF and EMM model data showed high performance of the neural network with a large amount of input data. Further testing and improvement of the neural network model is in progress.

FUNDING

The research was carried out within the framework of the state assignment of the Institute.

REFERENCES

1. *Kolesova V.I.* Analytical methods of magnetic cartography. Moscow: Nauka, 1985.

2. *Kolesova V.I., Cherkaeva E.A.* Calculation of the components of the vector anomalous geomagnetic field from modular data. Preprint No. 46 (735), Moscow: IZMIRAN, 1987.

3. *Yanovsky B.M.* Earth magnetism. Leningrad: Leningrad State University Publishing House, 591 p. 1978.

4. *Abadi M. et al*. Tensorflow: Large-scale machine learning on heterogeneous distributed systems //arXiv preprint arXiv:1603.04467. https://doi.org/10.48550/arXiv.1603.04467. 2016.

5. *Alken P., Thébault E., Beggan C. D., et al.* International Geomagnetic Reference Field: the thirteenth generation // Earth, Planets and Space. V. 73. № 1. P. 1–25. https://doi.org/10.1186/s40623-020-01288-x. 2021.

6. *Barkhatov*, *N.A*., *Vorobjev*, *V.G*., *Revunov*, *S.E*. et al. Effect of solar dynamics parameters on the formation of substorm activity // Geomagn. Aeron. V. 57. P. 251–256. https://doi.org/10.1134/S0016793217030021. 2017

7. *Buchanan A., Finn C. A., Love J. J. et al.* Geomagnetic referencing—the real-time compass for directional drillers // Oilfield Review. V. 25. № 3. P. 32−47. 2013.

8. *Coskun U. H*., *Sel B*., *Plaster B*. Magnetic field mapping of inaccessible regions using physics-informed neural networks //Scientific Reports. V. 12. №. 1. P. 12858–12867. https://doi.org/10.1038/s41598-022-15777-4. 2022.

9. *Kaftan İ.* Interpretation of magnetic anomalies using a genetic algorithm // Acta Geophysica. V. 65. № 4. P. 627–634. https://doi.org/10.1007/s11600-017-0060-7. 2017.

10. *Kaji C. V., Hoover R. C., Ragi S.* Underwater Navigation using Geomagnetic Field Variations / 2019 IEEE Intern. Conference on Electro Information Technology (EIT). https://doi.org/10.1109/eit.2019.8834192. 2019.

11. *Kingma D. P.*, *Ba J.* Adam: A method for stochastic optimization //arXiv preprint arXiv:1412.6980. 2014.

12. *Krizhevsky A.*, *Sutskever I.*, *Hinton G. E.* Imagenet classification with deep convolutional neural networks //Advances in neural information processing systems. V. 25. P. 1097–1105. 2012.

13. *Lourenco J. S., Morrison H. F.* Vector magnetic anomalies derived from measurements of a single component of the field // Geophysics. V. 38, № 2. P. 359–368. doi:10.1190/1.1440346. 1973.

14. *Maus*, *S.*, An ellipsoidal harmonic representation of Earth's lithospheric magnetic field to degree and order 720, Geochem. Geophys. Geosyst., 11, Q06015, https://doi.org/10.1029/2010GC003026. 2010

15. *Montesinos F. G., Blanco-Montenegro I., Arnoso J.* Three-dimensional inverse modelling of magnetic anomaly sources based on a genetic algorithm // Physics of the Earth and Planetary Interiors. V. 253. P. 74–87. https://doi.org/10.1016/j.pepi.2016.02.004. 2016.

16. *Pollok S.*, *Bjørk R.*, *Jørgensen P. S.* Inverse design of magnetic fields using deep learning //IEEE Transactions on Magnetics. V. 57. №. 7. P. 1-4. https://doi.org/10.1109/TMAG.2021.3082431. 2021.

17. *Pollok S. et al*. Magnetic field prediction using generative adversarial networks //Journal of Magnetism and Magnetic Materials. V. 571. P. 170556–170565. https://doi.org/10.1016/j.jmmm.2023.170556. 2023.

18. *Virtanen P. et al.* SciPy 1.0: fundamental algorithms for scientific computing in Python //Nature methods. V. 17. №. 3. P. 261-272. https://doi.org/10.1038/s41592-019-0686-2. 2020.

19. *Ying X.* An overview of overfitting and its solutions //Journal of physics: Conference series. – IOP Publishing. V. 1168. P. 022022–022029. https://doi.org/10.1088/1742-6596/1168/2/022022. 2019.

20. The National Centers for Environmental Information. (2018). [Online]. Available: https://www.ngdc.noaa.gov/geomag/geomag.shtml

Table 1. Average non-convexity for the reconstructed components of the anomalous magnetic field in the plane using the numerical algorithm and the trained artificial neural network.

Size image at the output	$\boldsymbol{B}_x$ (numerical algorithm)	$\boldsymbol{B}_y$ (numerical algorithm)	$\boldsymbol{B}_x$ (neural network)	$\boldsymbol{B}_y$ (neural network)
40 × 40 px	$L = 0.1068$	$L = 0.1058$	$L = 0.0271$	$L = 0.0269$
20 × 20 px	$L = 0.0125$	$L = 0.0125$	$L = 0.0069$	$L = 0.0071$

Table 2. Average unconvexity for the reconstructed components of the anomalous in-plane magnetic field from the noisy data using the numerical algorithm and trained artificial neural network.

Size image at the output	$\boldsymbol{B}_x$ (numerical algorithm)	$\boldsymbol{B}_y$ (numerical algorithm)	$\boldsymbol{B}_x$ (neural network)	$\boldsymbol{B}_y$ (neural network)
40 × 40 px	$L = 0.7493$	$L = 0.8122$	$L = 0.0733$	$L = 0.0680$
20 × 20 px	$L = 0.1496$	$L = 0.1895$	$L = 0.0122$	$L = 0.0126$

Figure captions

Fig. 1. Schematic representation of the artificial neural network architecture for recovering the B_x- and B_y-components of the anomalous magnetic field from the known vertical B_z-component.

Fig. 2. The value of the mismatch function for the training data series and validation data series as a function of epoch number during the training of the artificial neural network

Fig. 3. Results of recovering the horizontal components of B_x and B_y (*a* - *b*) using the numerical algorithm and (*c* - *d*) using the trained artificial neural network.

Fig. 4. Results of recovering horizontal components B_x and B_y (*a*) from the noisy data of component B_z, (*b*) using trained artificial neural network and (*c*) using numerical algorithm.

Fig. 5. The study area in which (*a*) the anomalous magnetic field was selected and (*b*) the distribution of the vertical component B_z over the study area.

Fig. 6. The original anomalous magnetic field, the reconstructed anomalous magnetic field using the trained artificial neural network and the difference between the original and reconstructed components of (*a*) B_x and (*b*) B_y.

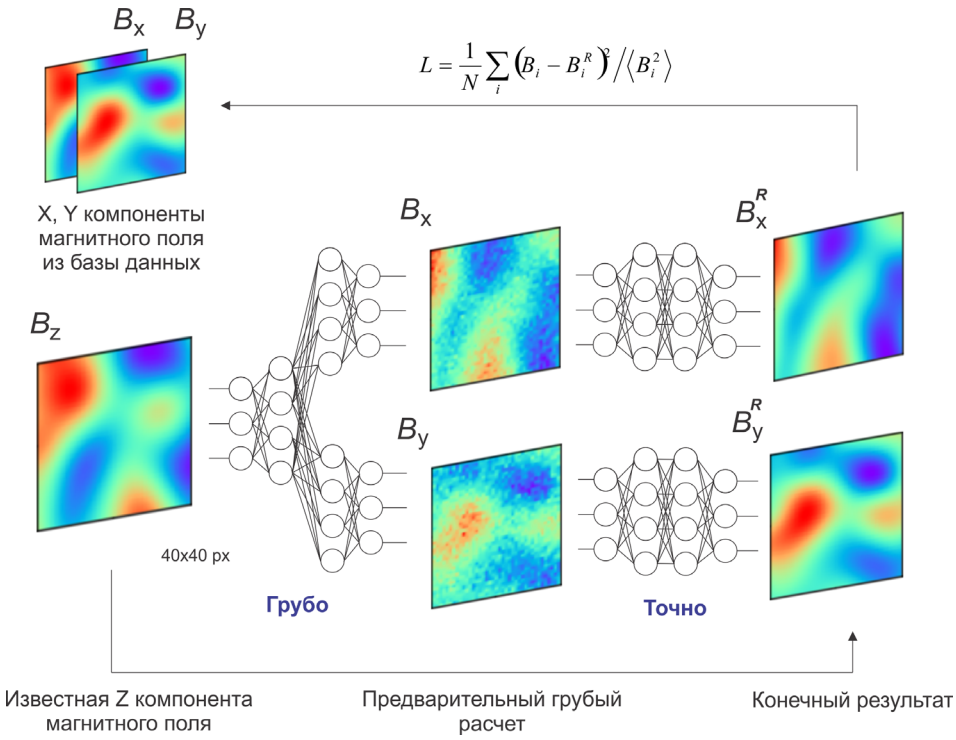
B_x B_y
$L = \frac{1}{N}\sum_i \left(B_i - B_i^R\right)^2 \Big/ \left\langle B_i^2 \right\rangle$
X, Y компоненты магнитного поля из базы данных
B_z
40x40 px
B_x
B_y
Грубо
B_x^R
B_y^R
Точно
Известная Z компонента магнитного поля
Предварительный грубый расчет
Конечный результат

Fig. 1.

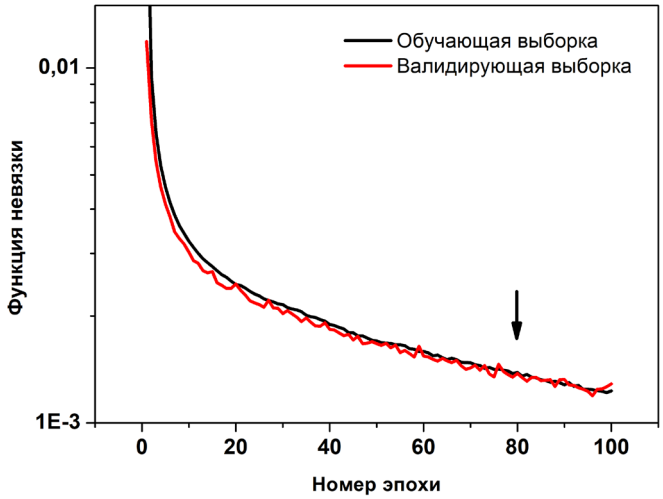
Обучающая выборка
Валидирующая выборка
0,01
1E-3
Функция невязки
0
20
40
60
80
100
Номер эпохи

Fig. 2.

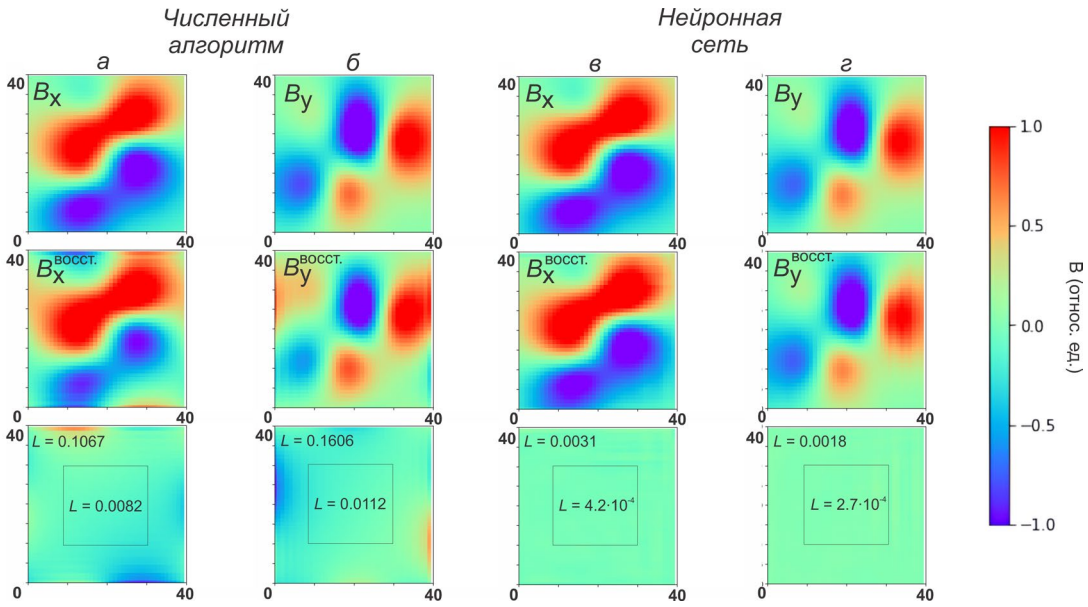
Численный алгоритм
Нейронная сеть
а
б
в
г
B_x
B_y
$B_x^{восст.}$
$B_y^{восст.}$
L = 0.1067
L = 0.0082
L = 0.1606
L = 0.0112
L = 0.0031
L = 4.2·10⁻⁴
L = 0.0018
L = 2.7·10⁻⁴
0
40
1.0
0.5
0.0
−0.5
−1.0
B (относ. ед.)

Fig. 3.

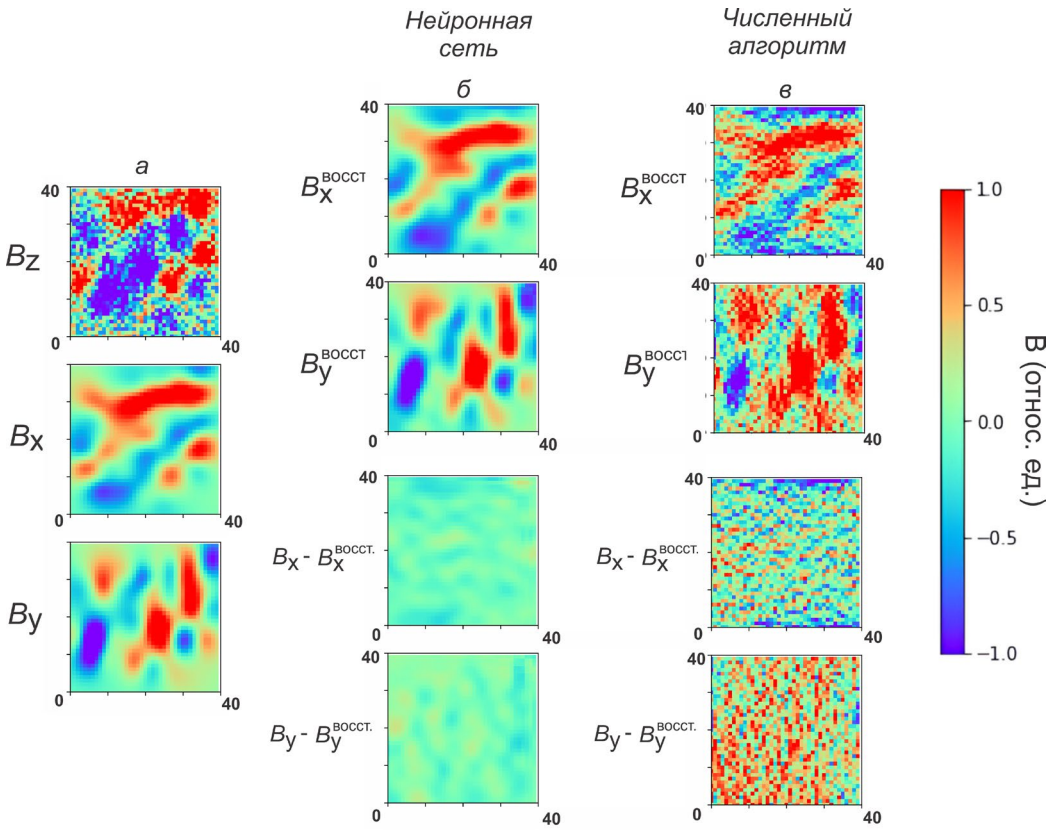
Нейронная сеть
Численный алгоритм
а
б
в
B_z
B_x
B_y
$B_x^{восст}$
$B_y^{восст}$
$B_x - B_x^{восст.}$
$B_y - B_y^{восст.}$
0
40
1.0
0.5
0.0
−0.5
−1.0
B (относ. ед.)

Fig. 4.

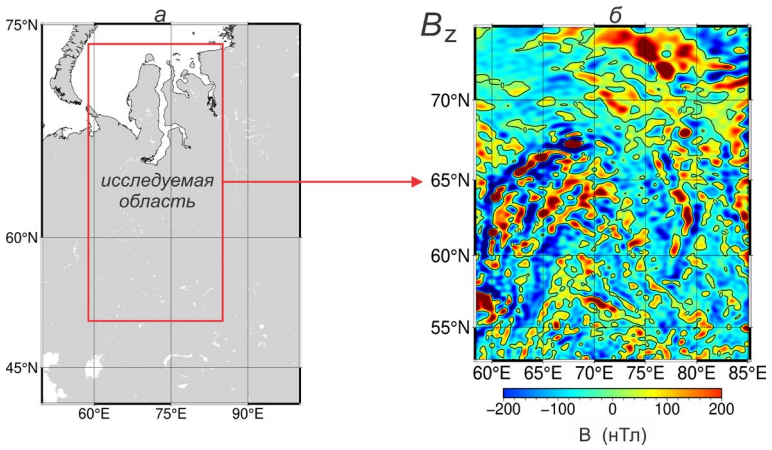
а
75°N
60°N
45°N
60°E
75°E
90°E
исследуемая
область
б
B_z
70°N
65°N
60°N
55°N
60°E 65°E 70°E 75°E 80°E 85°E
−200 −100 0 100 200
B (нТл)

Fig. 5.

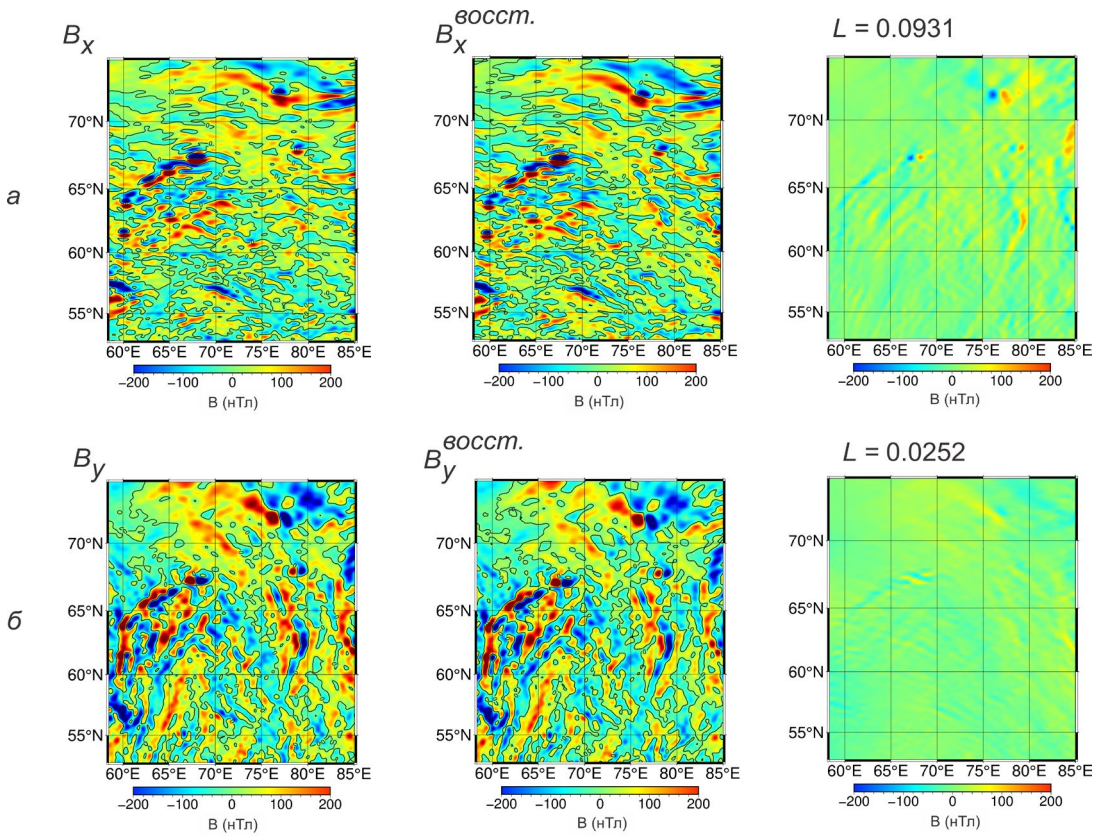
а
б
B_x
$B_x^{восст.}$
L = 0.0931
B_y
$B_y^{восст.}$
L = 0.0252
70°N
65°N
60°N
55°N
60°E 65°E 70°E 75°E 80°E 85°E
−200 −100 0 100 200
B (нТл)

Fig. 6.